Biomedical Analysis 1 (2024) 46–53

Contents lists available at ScienceDirect

Biomedical Analysis

journal homepage: www.keaipublishing.com/en/journals/bioana/

Dual-microRNA triggered and DNA-programmed nanomachine for subtype-based detection and tailored treatment of breast cancer cells

Shunmei Li, Xin Bi, Fang Yang, Ruo Yuan, Yun Xiang*

Key Laboratory of Luminescence Analysis and Molecular Sensing, Ministry of Education, School of Chemistry and Chemical Engineering, Southwest University, Chongqing 400715, PR China

A B S T R A C T

Discriminative detection and precise therapy targeting specific subtypes of breast cancers are critical for improving the treatment efficacy and thereby improving the survival rates of patients. Herein, we developed a dual-microRNA triggered DNA-programmed nanomachine for effective discrimination and modulated chemotherapy based on the subtypes of breast cancer cells. Two microRNA stimuli (miR-21 and miR-10b) can trigger the conformation change of the DNA nanomachine assembled on gold nanoparticles (AuNPs) through the toehold-mediated strand displacement reactions (TSDR), during which the fluorescence resonance energy transfer (FRET) signal is generated for microRNA imaging and the loaded doxorubicin (DOX) molecules are released for chemotherapy. The nanomachine can detect miR-10b as low as 0.047 nmol/L (S/N = 3) at a fixed concentration of miR-21 with high selectivity. Moreover, it allows effective discrimination of highly metastatic MDA-MB-231 breast cancer cells from non-metastatic MCF-7 breast cancer cells based on the dual microRNA expression patterns, and adjusts the DOX dosage according to the metastatic activity of cancer. This intelligent nanomachine with controlled release of anti-cancer drug in specific cancer cell subtypes can reduce the side effect to normal cells and facilitate the targeted therapy, which is promising as a theranostics nanoplatform in precise medicine.

Introduction

Breast cancer is the most common malignancy in women, posing a serious threat to the female health [1]. Due to the high inter-/intra-tumoral heterogeneity of breast cancer, clinical treatment and prognosis greatly vary in patients [2]. For example, the targeted therapy, such as endocrine therapy for the estrogen receptor-positive (ER^+) subtype and human epidermal growth factor receptor 2 (HER2)-targeted therapy for the $HER2^+$ subtype, has limited efficacy in treating the triple-negative breast cancer (TNBC) subtype with negative expression of progesterone (PR), ER, and HER2. Currently, chemotherapy is the main systemic treatment for TNBC [2]. Previous research showed that high-dose chemotherapy did improve overall survival (OS) in patients with TNBC while no OS benefit in unselected patients, compared with conventional-dose chemotherapy [3]. Treatment with the same strategy of high-dose chemotherapy without molecular subtyping often results in less efficiency and creates additional burden and pain for the patients [4]. Therefore, to improve treatment outcomes, prognosis and OS in breast cancer patients, precise molecular subtyping is paramount for guiding the administration of therapy [5]. Moreover, considering that multiple subtypes may coexist within a breast tumor, cancer diagnosis and treatment at single-cell level are highly promising for creating a new dimension in which precision medicine is tailored down to one cell and not only to the individual patient [5].

For the diagnosis and subtyping of breast cancer, histological examination of puncture biopsy sample is the “gold standard”, but it is invasive and difficult to realize dynamic monitoring of tumor progression and prognosis for treatment guidance [6]. In contrast,

* Corresponding author.
E-mail address: yunatswu@swu.edu.cn (Y. Xiang).

https://doi.org/10.1016/j.bioana.2024.01.001

2950-435X/© 2024 The Author(s). Publishing services by Elsevier B.V. on behalf of KeAi Communications Co. Ltd. This is an open access article under the CC BY-NC-ND license (http://creativecommons.org/licenses/by-nc-nd/4.0/).

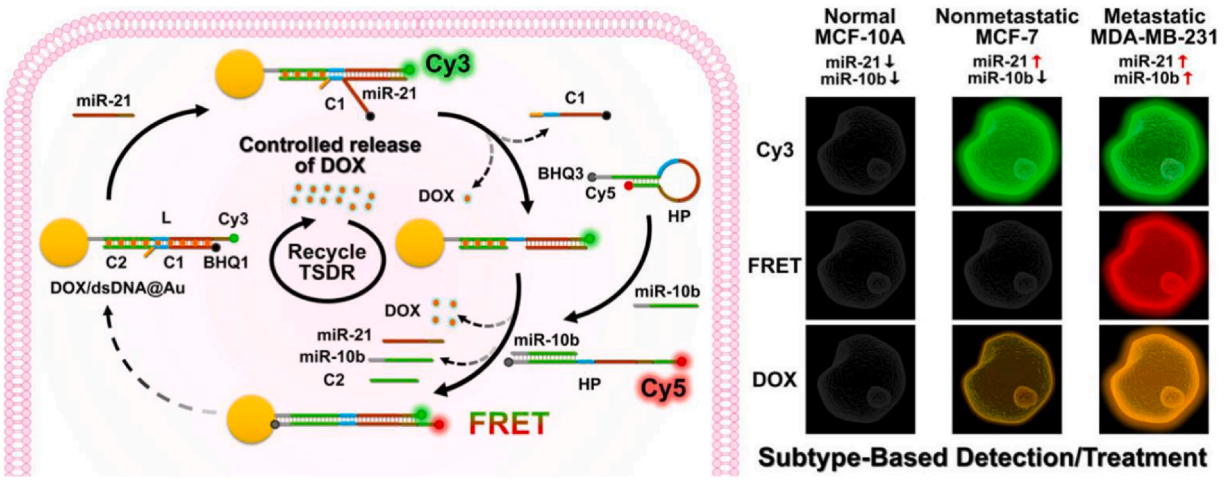

Fig. 1. Schematic illustration of the dual-miRNA triggered DNA-Au nanomachine based on toehold-mediated strand displacement reactions (TSDR) for controlled release of DOX, and the results of subtype-based detection and treatment.

fluorescence imaging techniques are capable of visualizing and monitoring minimal molecular changes occurring at early stage of cancers with high resolution and sensitivity [7]. For breast cancer imaging, various fluorescence probes have been explored based on detection of protein [8,9], microRNA (miRNA) [10,11] or pH [12]. Recently, miRNA, a class of small noncoding RNA, have attracted considerable attentions as emerging diagnostic and therapeutic biomarkers for cancers [13]. It has been revealed that the miRNA expression patterns are distinct in each intrinsic subtype of breast cancer cell [14], thereby offering not only high prediction accuracy for cancer subtype compared to single miRNA analysis,[15,16] but also improved therapeutic efficacy and accuracy at a single-cell level by serving as intracellular biomolecular stimuli for drug release [17]. Although, dual miRNA-triggered drug release for cancer therapy via the toehold-mediated strand displacement reactions (TSDR) has been proposed [18,19], the tailored treatment, such as high-dose chemotherapy in TNBC and conventional-dose chemotherapy in other breast subtype, has not been realized [20].

Herein, we proposed a dual-miRNA triggered DNA-programmed nanomachine for effective discrimination and tailored treatment of specific breast cancer cell types (Fig. 1). For proof-of-principle studies, two miRNAs, miR-21 and miR-10b, are employed as targets to initiate the DNA nanomachine through the TSDR, as their co-expression patterns are distinct in two typical breast cancer subtypes, the most common ER^+ subtype with high miR-21 but low miR-10b [21,22], and the most lethal TNBC subtype with overexpressed miR-21 and miR-10b [23,24]. The miR-21 is adopted to trigger the first TSDR and recover the Cy3 fluorescence, as well as releasing moderate dose of drug. After that, miR-10b is adopted to trigger the second TSDR and recycle the cascade TSDRs, which generates strong fluorescence resonance energy transfer (FRET) signal and releases a high-dose of drug. Consequently, the designed DNA nanomachine shows completely different fluorescence signal and drug release behavior after entering cells with different miRNA expression patterns, achieving subtype-based detection and tailored treatment of breast cancer cells, which holds great potential for precise molecular diagnosis and personalized therapy of breast cancer patients.

Experimental section

Reagents and materials

The used oligonucleotides (purified by HPLC, sequences see Table S1), diethyl pyrocarbonate (DEPC)-treated water, 1 × TE-buffer, Tris-HCl (pH 8.8) and 1 × Phosphate Buffered Saline (PBS, pH 7.4) buffer solutions were obtained from Sangon Biological Co. Ltd. (Shanghai, China). Doxorubicin hydrochloride, $HAuCl_4$, and $Na_3C_6H_5O_7{\cdot}2\,H_2O$ were obtained from Aladdin Reagent Co., Ltd. (Shanghai, China). Annexin V-FITC Apoptosis Detection Kit were ordered from Sigma-Aldrich (USA). The Lipo 3000 transfection kit, Dulbecco's modified Eagle's medium (DMEM), fetal bovine serum (FBS), and penicillin–streptomycin were purchased from Thermo Fisher Scientific (Shanghai, China). 3-(4,5-Dimethylthiazole)-2,5-diphenyltetrazolium bromide (MTT) and Hoechst 33342 kit were purchased from Beyotime Biotechnology (Shanghai, China). 0.45 μm PES filter was purchased from Tianjin Jinteng Co., Ltd (Tianjin, China). Phosphate buffer (PB) with different pH was prepared by mixing 100 mmol/L Na_2HPO_4 and 100 mmol/L NaH_2PO_4 solutions with different ratio. All other reagents were of analytical grade. The ultrapure water (18.2 MΩ·cm, Millipore Co., USA) was used in the experiments.

Instruments

Ultraviolet-visible (UV-Vis) absorption spectra were measured with UV-2750 UV-Vis spectrophotometer (Shimadzu, Japan). The fluorescence spectra were collected on F-7000 fluorescence spectrophotometer (Hitachi, Japan). Dynamic light scattering (DLS) and Zeta potential measurements were performed on the EliteSizer (Brookhaven, USA). Transmission electron microscopy (TEM) analysis

was performed on the FEI Tecnai G2 Spirit (Netherlands). The polyacrylamide gel electrophoresis (PAGE) analysis was photographed by a DigiGenius gel image system (Syngene, UK). The cytotoxicity test was measured on a microplate reader Molecular Devices M2 (Bio-Rad, USA). The confocal laser scanning microscopy (CLSM) images were obtained on a Zeiss LSM 710 confocal microscope. Flow cytometry data were analyzed on a Beckman Coulter Cytomic FC500 (USA).

Preparation of dsDNA

After adding 5 μL of 100 μmol/L L, 5 μL of 100 μmol/L C1, 5 μL of 100 μmol/L C2 and 35 μL of water, the mixture was heated at 95 °C for 5 min. And then the solution was slowly cooled to 37 °C and incubated for 3 h to form the dsDNA. The product was stored at 4 °C.

Preparation of AuNPs

A 0.01% (*w/v*) $HAuCl_4$ solution was prepared by adding 0.5 mL of 1% (*w/v*) $HAuCl_4$ solution into 49.5 mL water. Fifty microliters of 0.01% (*w/v*) $HAuCl_4$ solution was heated to 96 °C and then 1 mL of $Na_3C_6H_5O_7{\cdot}2\,H_2O$ solution (1%, *w/v*) was added into the solution under vigorous stirring. The mixture was stirred and heated for 30 min, and the color of the solution changed from light yellow to blue after several minutes, then changed to red after 20 min, and finally became purple red. The obtained solution was cooled to room temperature and filtered with 0.45 μm filter, then it was stored at 4 °C for further use.

Preparation of dsDNA@Au

The prepared AuNPs solution was concentrated to 1 nmol/L with centrifugation, and 250 nmol/L of dsDNA was added to the AuNPs solution at stored at 4 °C for 24 h. Next, PB solution (0.2 mol/L, pH = 7.4) was added to the above mixture to obtain a final phosphate concentration of 0.01 mol/L. NaCl solution (4 mol/L) was slowly added into the mixture in the next 48 h, and the final concentration of NaCl was 0.1 mol/L. The mixture was centrifuged at 13,500 r/min for 10 min to obtain a dark red precipitate, which was then dispersed in 0.01 mol/L PB solution and washed for three times. The dsDNA@Au solution was finally obtained after dispersing the product in PB solution with sonication.

The preparation of DOX/dsDNA@Au

1 mL of dsDNA@Au solution was mixed with various volume (2, 4, 6, 8, 10 μL) of 250 mmol/L DOX solution, and then the solution was shaken at 4 °C for 16 h. The obtained DOX/dsDNA@Au was centrifuged at 15,000 r/min for 10 min. The supernatant was used for the measurement of DOX loading rate. The precipitate was resuspended in water and stored at 4 °C for further use.

Cell culture

MCF-10A, MCF-7 and MDA-MB-231 cells were purchased from the Cell Resource Center of Shanghai Institute of Biological Sciences, Chinese Academy of Sciences. All the cells were cultured in DMEM (containing 5% fetal bovine serum and 1% penicillin–streptomycin) at 37 °C and 5% CO_2.

Confocal imaging analysis

MCF-10A, MCF-7 and MDA-MB-231 cells were plated on the glass slides in 48-well plates for 24 h. After being washed three times with PBS, the cells were incubated with dsDNA@Au or DOX/dsDNA@Au and HP-loaded liposome. The HP-loaded liposome was formed by mixing Lipo 3000 and HP (50 nmol/L) for 15 min. After 4 h of incubation, the cells were washed three times with PBS and subjected to CLSM imaging. Cy3 channel: λ_{ex} = 543 nm, λ_{em} = 560 – 630 nm; Cy5 channel: λ_{ex} = 633 nm, λ_{em} = 650 – 740 nm; FRET channel: λ_{ex} = 543 nm, λ_{em} = 650 – 740 nm; DOX channel: λ_{ex} = 488 nm, λ_{em} = 520 – 630 nm.

Flow cytometry experiments

MCF-10A, MCF-7 and MDA-MB-231 cells were seeded into 6-well plates at a density of 1×10^5 cells per well and incubated for 24 h. The cells were incubated with DOX/dsDNA@Au and HP-loaded liposome for 0, 2, and 4 h, then the cells were dissociated by 0.25% TrypsinEDTA (Life Technologies) and collected by centrifugation at 1000 r/min for 3 min. The cells were then washed twice with PBS, resuspended with 500 μL Annexin V-FITC binding buffer, and incubated with 10 μL of PI and 5 μL of Annexin V-FITC in dark for 10 min on ice. The rate of apoptosis was measured according to the protocol of the kit.

For the apoptosis induced by PBS, AuNPs, dsDNA@Au and DOX/dsDNA@Au, the cells were incubated with them separately for 4 h. Then the apoptosis rates were measured by a similar method.

Results and discussions

Principle of the DNA-Au nanomachine

In this DNA-Au nanomachine, the 5′-thiolate/3′-Cy3 dual-labeled linker DNA (L) is used to hybridize with 5′-BHQ1-modified probe DNA (C1) and the assistant probe DNA (C2), forming a double-stranded DNA (dsDNA) that is immobilized on gold nanoparticles (AuNPs) via Au–S bond. Doxorubicin (DOX) molecules are loaded into the intercalating G-C or C-G sites of the dsDNA [18]. In addition, a hairpin probe (HP) labelled with a pair of fluorophore (Cy5) and quencher (BHQ3) is designed for targeting miR-10b. When two miRNA targets are absent, no reaction occurs and the fluorescence of Cy3 and Cy5 is quenched. Once miR-21 exists, C1 is displaced due to the hybridization of miR-21 with the toehold region (purple color) on strand L (i.e., the first TSDR), resulting in the recovery of Cy3 fluorescence, the exposure of new toehold region (blue color) on L, and partial release of DOX due to the conformation change of the nanomachine [25]. Meanwhile, the presence of miR-10b opens the HP, separating the fluorophore and quencher, thus the fluorescence signal of Cy5 can be obtained. When miR-21 and miR-10b coexist, the exposed end of HP in the miR-10b/HP hybrid binds to the blue toehold region and triggers the branch migration (i.e., the second TSDR) to form the L/HP duplex, leading to the close proximity of Cy3 and Cy5 that generates FRET signal. In this second TSDR, miR-21 and miR-10b are released, accompanied with the release of the residual DOX in DNA-Au nanomachine. The regenerated miR-21 and miR-10b continue to trigger the next new cycle for amplifying the fluorescence signal and releasing large amount of DOX. Based on the dual miRNA expression patterns, the proposed nanomachine can discriminate different subtype of breast cancer cells and even intelligently adjust the DOX dosage in specific subtype.

Assembly of dsDNA@Au

The efficient assembly of dsDNA on AuNPs is one of the key factors of the proposed assay. First, the dsDNA formed by hybridization of strand L with C1 and C2 was verified by the native PAGE and fluorescence spectral analysis (Fig. 2A and S1). Next, AuNPs were synthesized using a sol-gel method [26], which showed regular spherical structure with well-dispersed distribution analyzed by TEM image (Fig. S2). UV-Vis absorption spectroscopy and DLS showed that the synthesized AuNPs had an absorption peak at 522 nm with a mean diameter of 24.0 ± 0.5 nm (Fig. S3). The dsDNA-functionalized AuNPs (dsDNA@Au) possessed two absorption peaks at 260 nm (ascribed to DNA) and 524 nm, with an increased diameter of 30.5 ± 2.2 nm. According to the Cy3 intensity in the supernatant of dsDNA@Au (Fig. S4), the ratio of dsDNA to AuNPs was optimized as 250:1, which possessed the

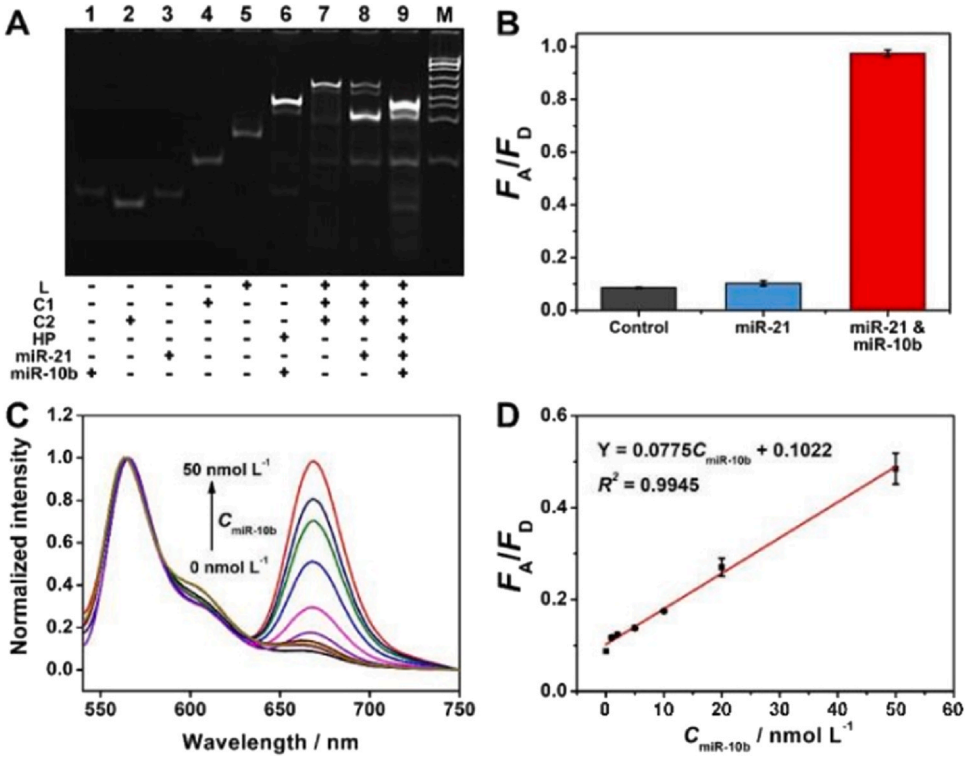

Fig. 2. (A) PAGE analysis of the strand displacement reactions. (B) Histogram of the F_A/F_D signals in response to PBS control, miR-21 and miR-21/miR-10b. (C) Fluorescence spectra of the nanomachine in response to different concentrations of miR-10b in the presence of 10 nmol/L miR-21 after normalized to F_D. (D) Plot of F_A/F_D vs miR-10b concentration.

highest loading rate of dsDNA calculated as 73.8% (corresponding to 184 dsDNA strands per AuNP). The above results demonstrated that the dsDNA was successfully immobilized onto AuNPs with high efficiency.

Feasibility of nanomachine

To evaluate the feasibility of this nanomachine, native PAGE was carried out to monitor the catalytic TSDR towards dual-miRNA triggers. As shown in Fig. 2A, incubating dsDNA with miR-21catalyst generated two new bands corresponding to the released C1 and the formed miR-21/L/C2 hybrid (lane 8), indicating that miR-21 can catalyze the first TSDR. Meanwhile, incubating HP with miR-10b catalyst generated a new band corresponding to the miR-10b/HP hybrid (lane 6). When miR-21 and miR-10b were added, the second TSDR was triggered, leading to the appearance of four new bands corresponding to the L/HP duplex and the released targets, C1 and C2 (lane 9). Furthermore, the feasibility of the TSDRs on the nanomachine for amplified detection of miRNA was tested with fluorescence spectroscopy. Incubating dsDNA@Au with miR-21 and HP with miR-10b can recover the fluorescence of Cy3 in L and Cy5 in HP, respectively (Figs. S5 and S6). After incubating dsDNA@Au and HP with miR-21 alone, negligible change of FRET signal (peak at 670 nm) was observed (Fig. S7), while the fluorescence intensity ratio of acceptor to donor (F_A/F_D) was greatly increased with the coexistence of miR-21 and miR-10b (Fig. 2B). All of these results verify the feasibility of the proposed DNA-Au nanomachine.

In vitro detection of miRNA

Prior to the fluorescence detection of miRNA using the proposed nanomachine, the reaction conditions were optimized including the reaction temperature and incubation time. The optimal conditions were obtained when the strand displacement reaction proceeded for 3 h at 37 °C (Figs. S8 and S9). As miR-21 was reported to be upregulated in various kinds of cancer cells [27], the concentration of miR-21 was fixed at a high concentration of 10 nmol/L, and the concentration of miR-10b varied from 0 to 50 nmol/L. As shown in Fig. 2C and 2D, the F_A/F_D signal increased with the increased concentration of miR-10b under the optimized condition. A linear relationship between F_A/F_D and miR-10b concentration was obtained at a range from 0.1 to 50 nmol/L ($R^2 = 0.994$) with a limit of detection (LOD) of 0.047 nmol/L ($S/N = 3$). In addition, the selectivity of this nanomachine was verified. By adding miR-21 and interference miRNAs (let-7 family) into the system, the F_A/F_D signal can only be generated by adding the miR-21 and miR-10b targets (Fig. S10), indicating a high selectivity of the proposed nanomachine.

Subtype discrimination of breast cells

The stability and cytotoxicity of the used probes are essential for biomedical applications. The PAGE images showed that the dsDNA and HP were stable in DMEM culture medium up to 6 h (Fig. S11). The 3-(4,5-dimethylthiazole)-2,5-diphenyltetrazolium bromide (MTT) assays showed that AuNPs and dsDNA@Au possessed negligible cytotoxicity (Fig. S12) for the normal MCF-10A cells (human mammary epithelial cell line), the non-metastatic MCF-7 cells (human ER^+ breast cancer cell line), and the highly metastatic MDA-MB-231 cells (human triple-negative breast cancer cell line). These results indicate a satisfactory stability and cytocompatibility of the nanomachine. To investigate the specific response of the nanomachine to the dual miRNA targets in living cells, HP was transfected by commercial liposome, while dsDNA@Au was directly internalized into cells through endocytosis. As shown in CLSM images (Fig. 3), after 4 h of incubation, strong Cy3, Cy5 and FRET signals were observed in MDA-MB-231 cells with overexpressed

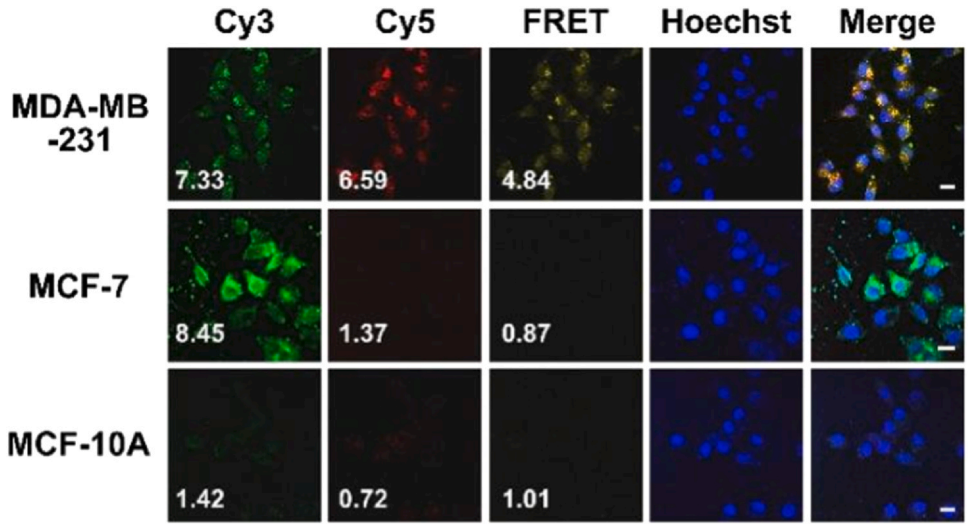

Fig. 3. CLSM images and the corresponding fluorescence intensity of MDA-MB-231, MCF-7 and MCF-10A cells incubated with the DNA nanomachine (dsDNA@Au and HP used here) for 4 h. Scale bar = 20 μm.

miR-21 and miR-10b [23,24]. In comparison, the Cy3 signal was strong while Cy5 and FRET signals were negligible in MCF-7 cells. This should be ascribed to the upregulated miR-21 level in MCF-7 cells that triggered the first TSDR and recovered the Cy3 fluorescence, while the lower expression of miR-10b in MCF-7 cells compared to that in MDA-MB-231 cells cannot efficiently open HP to trigger the second TSDR [28], which resulted in lower Cy5 and FRET intensity. However, in MCF-10A cells that were reported with downregulated miR-21 and miR-10b [29], the Cy3, Cy5 and FRET signals were not visible. The above results confirm that the nanomachine was specifically triggered by intracellular miR-21 and miR-10b, facilitating the discrimination between the non-metastatic MCF-7 cells and the highly metastatic MDA-MB-231 cells.

Loading and in vitro release of DOX

The exceptional responsiveness of the stable and biocompatible DNA-Au nanomachine to dual miRNA stimuli makes it an ideal candidate for controllable drug delivery. First, the loading of DOX into dsDNA@Au was verified. The DOX loaded dsDNA@Au (DOX/dsDNA@Au) showed three absorption peaks at 260, 480, and 524 nm, corresponding to dsDNA, DOX, and AuNPs, respectively (Fig. S13A). After loading the positively charged DOX molecules, the Zeta potential of dsDNA@Au changed from −27.0 mV to 2.0 mV (Fig. S13B). The fluorescence of DOX was efficiently quenched after being loaded into dsDNA@Au (Fig. S14). The loading concentration reached equilibrium at incubating 2.0 μmol/L DOX with dsDNA@Au. According to the standard curve of DOX (Fig. S15), the average number of DOX molecules loaded on each dsDNA@Au was estimated to be 1745, which is superior to other reported DOX loading efficiency in DNA-Au complex [30]. The release behaviors of DOX from DOX/dsDNA@Au triggered by dual miRNA stimuli were also investigated in vitro. As shown in Fig. S16, significant fluorescence recovery of DOX was observed in the presence of miR-21 and miR-10b. These results suggest the high drug release efficiency of the nanomachine in response to the dual miRNAs, which can serve as an efficient candidate for intracellular drug delivery allowing effective treatment of specific cancer cell types based on expression patterns of miRNAs.

Subtype-based tailored treatment

Theoretically, the DOX can be released depending on the molecular subtype of cancer cells. Therefore, the drug release of DOX/dsDNA@Au in living cells was investigated by CLSM analysis (Fig. 4A). After treatment with DOX/dsDNA@Au and HP, the DOX signal in MCF-7 and MDA-MB-231 cells was 3.0 and 11.6 times that in MCF-10A cells, respectively. The above results showed that this nanomachine can intelligently release DOX depending on the concentration of dual-miRNAs, achieving slight DOX release in non-metastatic cancer cells and strong DOX release in highly metastatic cancer cells.

The increasing dose of DOX should results in increasing cytotoxicity. Therefore, the apoptosis of MCF-10A, MCF-7 and MDA-MB-231 cells after treatment with the nanomachine (including DOX/dsDNA@Au and HP) was measured by flow cytometry using Annexin V-FITC and propidium iodide (PI) staining. As shown in Fig. 4B, the apoptosis rates of MCF-10A cell were 4.1%, 3.3% and 7.8% at 0, 2 and 4 h, respectively, indicating a very low cytotoxicity of the nanomachine towards normal MCF-10A cells. Meanwhile, the apoptosis rates of MCF-7 cells were 10.9%, 16.0% and 21.3% at 0, 2 and 4 h, indicating a moderate cytotoxicity of the nanoplatform

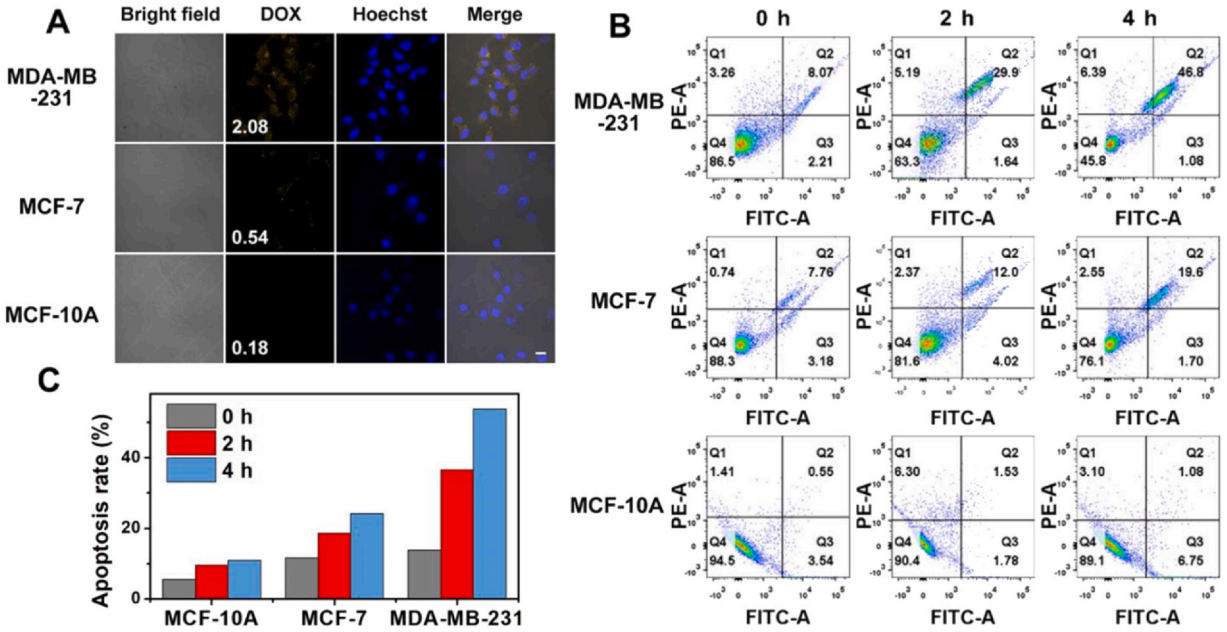

Fig. 4. (A) CLSM images and the corresponding DOX intensities of MCF-10A, MCF-7 and MDA-MB-231 cells incubated with the DNA nanomachine for 4 h. Scale bar = 20 μm. (B) The apoptosis of MCF-10A, MCF-7, MDA-MB-231 cells with the DNA nanomachine. (C) Histogram of apoptosis rate of different cells over time.

towards the non-metastatic breast cancer cells. In contrast, the apoptosis rates were 10.3%, 31.6% and 47.9% at 0, 2 and 4 h for the miR-21/miR-10b-upregualted MDA-MB-231 cells. As shown in Fig. 4C, the apoptosis rate was increased with increasing metastatic activity of cancer cells, while kept in a low level for the normal cells. This controlled release of anti-cancer drug in specific cancer cell subtypes can reduce the side effect to normal cells and facilitate the targeted therapy, which is essential for precise medicine. In addition, the apoptosis induced by AuNPs, dsDNA@Au and free DOX for MDA-MB-231 cells were also investigated (Fig. S17). After 4 h of incubation, PBS control, AuNPs and dsDNA@Au only induced an apoptosis rate of 8.8%, 10.1% and 11.0%, respectively, indicating that the AuNP nanocarriers have a high biocompatibility, and the apoptosis caused by the nanomachine should be attributed to the loaded DOX. Furthermore, the free DOX only induced an apoptosis rate of 24.8%, which is lower than that of the nanomachine (47.9%). This can be ascribed to the possible alterations of DOX delivery route by the nanomachine to bypass P-glycoprotein-mediated drug efflux and thus increase treatment efficacy in contrast to the free DOX [17,31]. All the above results have preliminarily demonstrated the dual-miRNA triggered therapy performance of our nanomachine, and the encouraging results would inspire us to apply this powerful theranostics tool in animal model in the future.

Conclusion

In summary, we developed an intelligent DNA-Au nanomachine triggered by two endogenous cancer metastasis-related miRNAs to serve as a theranostics nanoplatform for effective discrimination and targeted therapy of specific breast cancer cell types. In this proposed assay, the amplification reaction can only occur with the simultaneous trigger of miR-21 and miR-10b, resulting in the superior sensitivity and selectivity of the nanomachine for dual-miRNA imaging in living cells. More importantly, the loaded DOX in the nanomachine can be released during the amplification reaction, whose dosage is positively correlated with the dual-miRNA expression patterns, i.e., the metastatic activity of breast cancer cells. With the intelligent design of the nanomachine, the non-metastatic MCF-7 cells (ER^+ breast cancer cell line with overexpression of miR-21) and the highly metastatic MDA-MB-231 cells (triple-negative breast cancer cell line with overexpression of miR-21 and miR-10b) can be discriminated and receive moderate and maximum DOX dosage, respectively. This proposed nanomachine holds promise to function as a theranostics nanoplatform for dynamic monitoring of tumor progression, specific diagnosis, targeted therapy in various cancer cells with distinct biomarkers of genes, proteins, and RNAs.

Declaration of Competing Interest

The authors declare no competing financial interest.

Acknowledgments

This work was supported by the National Natural Science Foundation of China (No. 22174112).

Supporting information

The experimental details, the sequences of the used oligonucleotides, the fluorescence spectra of L and dsDNA, the TEM image of AuNPs, the UV-Vis absorption spectra and DLS results of the components, the loading of dsDNA by AuNPs, the fluorescence response of dsDNA@Au, HP and nanomachine towards miR-21 and miR-10b, the optimization of incubation time and temperature, the selectivity of the dsDNA@Au, the stability and cytotoxicity of dsDNA@Au, the loading and releasing of DOX by dsDNA@Au, the apoptosis induced by different components.

Appendix A. Supporting information

Supplementary data associated with this article can be found in the online version at doi:10.1016/j.bioana.2024.01.001.

References

[1] R.L. Siegel, K.D. Miller, H.E. Fuchs, A. Jemal, CA-Cancer J. Clin. 71 (1) (2021) 7–33.
[2] L. Yin, J.J. Duan, X.W. Bian, S.C. Yu, Breast Cancer Res. 22 (1) (2020) 13.
[3] D.A. Berry, N.T. Ueno, M.M. Johnson, J. Clin. Oncol. 29 (24) (2011) 3214.
[4] A. Matikas, T. Foukakis, V. Moebus, R. Greil, N.O. Bengtsson, G.G. Steger, M. Untch, H. Johansson, M. Hellström, P. Malmström, M. Gnant, S. Loibl, J. Bergh, Ann. Oncol. 30 (1) (2019) 109–114.
[5] S.K. Yeo, J.L. Guan, Trends Cancer 3 (11) (2017) 753–760.
[6] Y. Cao, X. Yu, T. Zeng, Z. Fu, Y. Zhao, B. Nie, J. Zhao, Y. Yin, G. Li, J. Am. Chem. Soc. 144 (30) (2022) 13475–13486.
[7] Q. Li, S. Li, S. He, W. Chen, P. Cheng, Y. Zhang, Q. Miao, K. Pu, Angew. Chem. Int. Ed. 132 (18) (2020) 7084–7089.
[8] Y. Sun, X. Zhou, L. Sun, X. Zhao, Y. He, G. Gao, W. Han, J. Zhou, Chin. Chem. Lett. 33 (9) (2022) 4229–4232.
[9] D.D. Yang, M. Liu, J. Xu, C. Yang, X.X. Wang, Y.B. Lou, N.Y. He, Z.F. Wang, Talanta 185 (2018) 113–117.
[10] X. Huang, Y. Zhang, J. Chen, L. Zhang, Y. Xu, W. Yin, Y. Shi, S.Y. Liu, X. Zou, Z. Dai, Anal. Chem. 94 (35) (2022) 12221–12230.
[11] L. Yang, S. Yu, Y. Yan, S. Bi, J.J. Zhu, Anal. Chem. 94 (19) (2022) 7075–7083.
[12] D. Yue, M. Wang, F. Deng, W. Yin, H. Zhao, X. Zhao, Z. Xu, Chin. Chem. Lett. 29 (5) (2018) 648–656.
[13] F.J. Nassar, R. Nasr, R. Talhouk, Pharmacol. Ther. 172 (2017) 34–39.
[14] L. Qiao, C. Wu, Z. Cai, X. Wu, P. Wu, C. Cai, Anal. Chim. Acta 1093 (2020) 86–92.
[15] R. Yue, Z. Li, G. Wang, J. Li, N. Ma, ACS Sens. 4 (1) (2019) 250–256.

[16] J.Y. Jang, Y.S. Kim, K.N. Kang, K.H. Kim, Y.J. Park, C.W. Kim, Mol. Clin. Oncol. 14 (2) (2021) 31–41.
[17] X. Luo, Z. Li, G. Wang, X. He, X. Shen, Q. Sun, L. Wang, R. Yue, N. Ma, ACS Appl. Mater. Interfaces 9 (39) (2017) 33624–33631.
[18] R. Yue, M. Chen, N. Ma, ACS Appl. Mater. Interfaces 12 (29) (2020) 32493–32502.
[19] Y. Guo, B. Wei, S. Xiao, D. Yao, H. Li, H. Xu, T. Song, X. Li, H. Liang, Quant. Biol. 5 (2017) 25–41.
[20] F.C. Simmel, B. Yurke, H.R. Singh, Chem. Rev. 119 (10) (2019) 6326–6369.
[21] L. Ma, J. Teruya-Feldstein, R.A. Weinberg, Nature 449 (7163) (2007) 682–688.
[22] H. Wang, Z.Q. Tan, H. Hu, H.Z. Liu, T.W. Wu, C. Zheng, X.L. Wang, Z.Z. Luo, J. Wang, S.Y. Liu, Z.X. Lu, J.C. Tu, BMC Cancer 19 (1) (2019) 13.
[23] H. Fang, J.P. Xie, M. Zhang, Z.W. Zhao, Y. Wan, Y.Q. Yao, Am. J. Transl. Res. 9 (3) (2017) 953.
[24] L. Ma, Breast Cancer Res. 12 (5) (2010) 1–5.
[25] S. Yu, Y. Zhou, Y. Sun, S. Wu, T. Xu, Y.C. Chang, S. Bi, L.P. Jiang, J.J. Zhu, Angew. Chem. Int. Ed. 60 (11) (2021) 5948–5958.
[26] P. Zhao, N. Li, D. Astruc, Coord. Chem. Rev. 257 (3-4) (2013) 638–665.
[27] D. Bautista-Sanchez, C. Arriaga-Canon, A. Pedroza-Torres, I.A. De La Rosa-Velazquez, R. Gonzalez-Barrios, L. Contreras-Espinosa, R. Montiel-Manriquez, C. Castro-Hernandez, V. Fragoso-Ontiveros, R.M. Alvarez-Gomez, L.A. Herrera, Mol. Ther. - Nucl. Acids 20 (2020) 409–420.
[28] N. Haghnavaz, F. Asghari, N. Shekari, D. Shanehbandi, M. Javadian, A. Mohammadi, B. Baradaran, T. Kazemi, Middle East J. Cancer 11 (1) (2020) 42–49.
[29] Z.S. Hashemi, M. Forouzandeh Moghadam, S. Khalili, M. Ghavami, F. Salimi, E. Sadroddiny, Breast Cancer 26 (2019) 215–228.
[30] G.Y. Sun, Y.C. Du, Y.X. Cui, J. Wang, X.Y. Li, A.N. Tang, D.M. Kong, ACS Appl. Mater. Interfaces 11 (16) (2019) 14684–14692.
[31] D. Goren, A.T. Horowitz, D. Tzemach, M. Tarshish, S. Zalipsky, A. Gabizon, Clin. Cancer Res. 6 (5) (2000) 1949–1957.